The Astrophysical Journal, 856:120 (9pp), 2018 April 1 https://doi.org/10.3847/1538-4357/aab356

Coronal Proerties of the Seyfert 1 Galaxy 3C 120 with *NuSTAR*

Priyanka Rani and C. S. Stalin
Indian Institute of Astrophysics, Koramangala, Bangalore 560034, India; priyanka@iiap.res.in
Received 2017 April 14; revised 2018 February 22; accepted 2018 February 26; published 2018 March 30

Abstract

We present a measurement of the cut-off energy, a proxy for the temperature of the corona in the nuclear continuum of the Seyfert 1 galaxy 3C 120 using ∼120 ks of observation from *NuSTAR*. The quality broadband spectrum from 3–79 keV enabled us to measure the Compton reflection component (R) and to constrain the temperature of the coronal plasma. Fitting one of the advanced Comptonization models, *compPS*, to the observed broadband spectrum, we derived the kinetic temperature of the electrons in the corona to be $kT_e = 25 \pm 2$ keV with a Compton y parameter of $y = 2.2 \pm 0.1$ for a slab geometry and $kT_e = 26^{+2}_{-0}$ keV with a y of $2.99^{+2.99}_{-0.18}$ assuming a spherical geometry. We noticed excess emission from ∼10–35 keV arising due to Compton reflection and a broad Fe Kα line at 6.43 keV with an equivalent width of 60 ± 5 eV. The variations in count rates in the soft (3–10 keV) band are found to be larger compared to the hard (10–79 keV) band, with mean fractional variability amplitudes of 0.065 ± 0.002 and 0.052 ± 0.003 for the soft and hard bands respectively. 3C 120 is known to have a strong jet; however, our results indicate that it is either dormant or its contribution, if any, to the X-ray emission is negligible during the epoch of *NuSTAR* observation.

Key words: galaxies: active – galaxies: Seyfert – quasars: individual (3C120)

1. Introduction

Active galactic nuclei (AGNs) are energetic extragalactic sources believed to be powered by a complex physical process, namely the accretion of matter on to supermassive black holes (SMBHs) residing at the centers of galaxies (Rees 1984). The matter accreted by the SMBH forms an optically thick, geometrically thin accretion disk (Shakura & Sunyaev 1973), with a temperature of about 10^4–10^5 K for an SMBH of mass 10^6–$10^9\,M_\odot$, and that emits predominantly in the optical/UV region of the electromagnetic spectrum. The components of an AGN therefore include an accretion disk surrounding the central SMBH, an X-ray-emitting corona, an obscuring torus surrounding the accretion disk and a relativistic jet in about 15% of AGNs (Urry & Padovani 1995). While the accretion disk emits in the optical/UV bands, the observed hard X-ray continuum is believed to be caused by thermal Comptonization of the accretion disk photons in a hot (∼10^9 K), optically thin corona (Haardt & Maraschi 1991; Haardt et al. 1994, 1997) in the radio-quiet category (those without radio jets) of AGNs. This Comptonization process gives rise to the observed power-law X-ray spectrum in AGNs and the shape of this observed spectrum depends on the seed photon field, the kinetic temperature of the plasma kT_e, the optical depth τ, and the geometry of the corona. Arguments in the literature indicate the corona to lie between 3–10 R_g above the central SMBH (Fabian et al. 2009). Here, $R_g = GM/c^2$ is the gravitational radius of an SBMH with mass $M_{\rm BH}$. In addition to the primary power-law continuum, the X-ray spectrum also contains a Fe Kα line at 6.4 keV. The origin of this line, unambiguously detected for the first time in the source MCG-6-30-15 (Tanaka et al. 1995), is attributed to the reflection of the power-law photons from the hot corona by the relatively cold accretion disk (George & Fabian 1991). This line is now observed in many AGNs (Miller 2007). Therefore, X-ray observations of AGNs provide very important clues to the physical processes that occur close to the SMBH.

A feature in the hard X-ray spectra of AGNs that arises from the thermal Comptonization process is the presence of a high-energy cut off ($E_{\rm cut}$) which is related to the plasma electron temperature (kT_e) of the corona, which is found to range between 50 and 100 keV. Measurements of $E_{\rm cut}$ for about 100 AGNs (Petrucci et al. 2001; Dadina 2007; Marinucci & Tortosa 2016) are currently available based on observations using older observatories such as the *Compton Gamma Ray Observatory* (*CGRO*; Zdziarski et al. 2000), *BeppoSAX* (Perola et al. 2002), and the currently operating satellite *INTEGRAL* (Malizia et al. 2014). For example, Dadina (2007), using *BeppoSAX* data in the energy range 2–100 keV, has provided $E_{\rm cut}$ measurements for 34 sources and lower limits for 54 others. Also, Malizia et al. 2014, using data from *XMM*, *INTEGRAL*, and *Swift*, has provided $E_{\rm cut}$ values for 26 AGNs and lower limits for 11 others. Most of these measurements have large error bars, which may be due to the quality of the data, as well as the degeneracy that is known to prevail between $E_{\rm cut}$ and other physical properties of the sources such as the slope of the primary X-ray power law and the amount of radiation that is Compton up-scattered by the circumnuclear material (Marinucci & Tortosa 2016).

One of the important physical parameters of the Comptonizing corona in an AGN is its plasma temperature, kT_e. The value of kT_e in many instances is indirectly obtained by fitting simple phenomnological models such as the cut-off power law to the observed X-ray spectrum to find $E_{\rm cut}$ and subsequently kT_e is deduced using certain approximations. However, kT_e values are available for many AGNs based on physical model fits to AGN spectra (Petrucci et al. 2001; Lubiński et al. 2016). Disentangling the different spectral components that are present in the X-ray spectra of AGNs and constraining their characteristic parameters require high signal-to-noise ratio (S/N) data covering a wide energy range. These limitations are now overcome to a large extent owing to the availability of the focusing hard X-ray telescope, the *Nuclear Spectroscopic Telescope Array*, *NuSTAR* (Harrison et al. 2013), due to its high sensitivity and wide energy coverage from 3–79 keV.

However, *NuSTAR* can provide precise measurements only for sources with $E_{\rm cut} < 150$ keV (Malizia et al. 2014). Measurements beyond this from *NuSTAR* will not be reliable due to its own lack of effective area beyond 79 keV. Using *NuSTAR*, $E_{\rm cut}$ as well as the more physical coronal plasma temperature kT_e has been measured in about a dozen AGNs (Ballantyne et al. 2014; Brenneman et al. 2014a; Marinucci et al. 2014; Baloković 2015; Lohfink et al. 2015, 2017; Matt et al. 2015; Kammoun et al. 2017; Kara et al. 2017; Pahari et al. 2017; Tortosa et al. 2017) and also summarized by Marinucci & Tortosa (2016). Though *NuSTAR* observations have enabled us to characterize the coronal properties of about a dozen AGNs, to have a complete knowledge of the geometrical and physical properties of the X-ray corona in AGNs, there is a need to extend such studies on the X-ray properties to a large sample.

In this paper, we present the results of our analysis of X-ray data on 3C 120 observed by *NuSTAR* for a total duration of about 120 ks. 3C 120 is an X-ray-bright Seyfert 1 galaxy at $z = 0.033$ (Burbidge 1967), having a black hole mass of $5.6 \times 10^7\ M_\odot$ (Bentz & Katz 2015). It is also classified as a broad line radio galaxy (BLRG) by Walker et al. (1987). It has a radio morphology similar to the Fanaroff Riley Class I (FRI) category of AGNs (Fanaroff & Riley 1974). Its one-sided jet has an inclination to the line of sight of $\sim 14^\circ$ (Eracleous & Halpern 1998) which is based on the apparent superluminal speed $\beta_{\rm app}$ reported by Zensus (1989). The jet is known to extend on scales up to 100 kpc (Walker et al. 1987). It has been found to be variable in X-rays. A broad Fe Kα line well fitted by a Gaussian with a σ of 0.8 keV and having an equivalent width of 400 eV has been found from ASCA observations (Halpern 1985). It has not been detected in γ-rays by the *CGRO* (Lin et al. 1993). However, using data from the Oriented Scintillation Spectroscopy Experiment (OSSE; Johnson et al. 1993) on board the *CGRO*, Wozniak et al. (1998) found the presence of a spectral break in 3C 120 between X-rays and soft γ-rays. 3C 120 was detected by *Fermi* using the first 15 months of data (Abdo et al. 2010), but not detected in the second *Fermi*-LAT catalog (2FGL; Nolan et al. 2012) or the third *Fermi*-LAT catalog (3FGL; Acero et al. 2015), indicating that the source is variable in the high-energy γ-rays. Using 180 and 365 day binning on the data obtained between 2008 August–2013 December, Sahakyan et al. (2015) found γ-ray flux variations. Using a 5 day binned light curve, Tanaka et al. (2015) noticed that 3C 120 was detected only at certain epochs.

In this work, we focus on both the timing and broadband (3–79 keV) spectral analysis. Though 3C 120 has been studied for flux variability as part of the analysis of a large sample of AGNs by Rani et al. (2017), analysis of the broadband X-ray data to constrain its coronal properties using *NuSTAR* has been carried out for the first time. From *BeppoSAX* observations, Zdziarski & Grandi (2001) have estimated an $E_{\rm cut}$ of 100–300 keV. Also, Wozniak et al. (1998), using the average OSSE spectrum together with ASCA data, reported a $E_{\rm cut}$ of 130^{+150}_{-40} keV. Using data from several telescopes Lubiński et al. (2016) obtained a value of $kT_e = 176^{+24}_{-23}$ keV. This paper is organized as follows. In Section 2 we report on the *NuSTAR* observations and data reduction. In Section 3 we present the analysis of the *NuSTAR* data. The results are discussed in Section 4 followed by the summary in the final section.

2. Observation and Data Reduction

3C 120 was observed by *NuSTAR* (Harrison et al. 2013) on 2013 February 6 (ObsID 60001042003) for 127 ks in the 3–79 keV band. The data were reduced using the *NuSTAR* Data Analysis Software package *NuSTARDAS* v.1.6.0 distributed by the High Energy Astrophysics Archive Research Center (HEASARC). We generated the cleaned and screened event files, taking also into account the passage of the satellite through the South Atlantic Anomaly using the *nupipeline* task and using CALDB 20161207. A circular region of radius 60″ was taken centered on the peak of the source image to extract the source spectrum and light curve. To extract the background spectrum and light curve we again selected a circular region of radius 60″ away from the source on the same detector. Light curves were generated with 300 s binning in the 3–79 keV band for both the focal plane modules, FPMA and FPMB. They were further divided into soft (3–10 keV) and hard (10–79 keV) bands. To get the final light curves, the count rates from the two modules FPMA and FPMB were combined using the *lcmath* task in FTOOLS V6.19.

We generated the source and background spectra and response files in the energy range of 3–79 keV in both FPMA and FPMB using the *nuproducts* package available in *NuSTARDAS*. Instead of combining the spectra or responses from FPMA and FPMB, we fitted them simultaneously, allowing the cross normalization for both modules to vary freely in all fits. We used *XSPEC* (version 12.9.0; Arnaud 2014) for all spectral analysis. During the various model fits in *XSPEC*, we used the Anders & Grevesse (1989) set of solar abundances and the Balucinska-Church & McCammon (1992) photoelectric cross sections. The χ^2 minimization technique in *XSPEC* was used to get the best model description of the data and all errors were calculated using the $\chi^2 = 2.71$ criterion, i.e., 90% confidence level.

To check for any possible effects on our choice of the background region used to get the light curves and the source spectrum, we also used a background found in an annular region around the source having an inner radius of 50 pixels and an outer radius of 80 pixels (1 pixel = 2.46 arcsec). The mean count rates of the source light curve in the 3–79 keV band using the background taken from the circular region away from the source and using the annular region surrounding the source are 3.88 ± 0.20 and 3.84 ± 0.20 respectively. The choice of the background thus has a neglible effect on the light curves presented here. Similarly, the average fluxes of the source in the 3–79 keV band obtained from a simple power-law fit to the spectrum are $(1.372 \pm 0.007) \times 10^{-10}$ and $(1.237 \pm 0.007) \times 10^{-10}$ erg s^{-1} cm^{-2} respectively using the background taken from the circular region away from the source and the annular region surrounding the source. The difference in the fluxes deduced from the spectra using two choices of the background selection is less than 10%. Thus, the selection of background region has no significant impact on the spectral and timing analysis carried out on 3C 120.

3. Analysis of the Data

3.1. Flux Variability

In Figure 1 we show the light curves in the two energy bands, 3–10 keV and 10–79 keV, as well the hardness ratio (HR) curve. The HR is evaluated as the ratio between the count rates in the 10–79 keV to 3–10 keV bands. The source is found

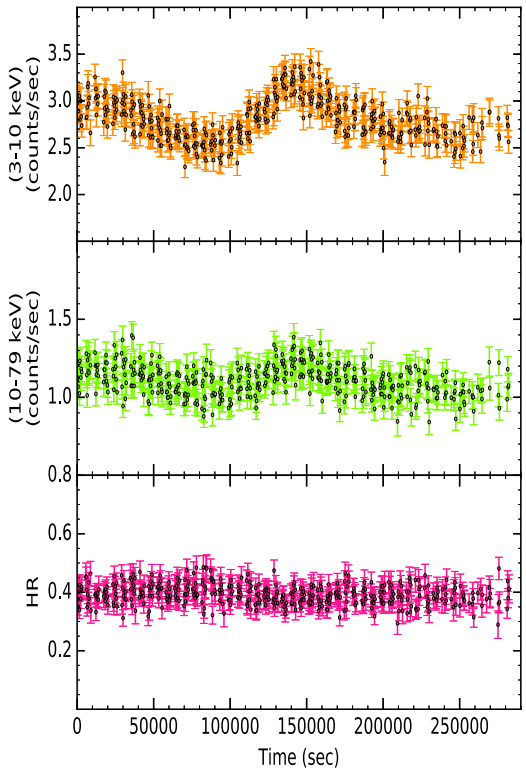

Figure 1. Light curves in counts s^{-1} for the soft (top) and hard (middle) bands. The zero point of the time axis is 2013-02-06T23:51:07. The variation of HR is shown on the bottom panel.

to show variations in both the soft and hard bands. To characterize the flux variations from observed count rates, we used the fractional root mean square variability amplitude ($F_{\rm var}$), which gives an estimate of the intrinsic variability amplitude relative to the mean count rate (Edelson et al. 2002; Vaughan et al. 2003). We found $F_{\rm var}$ values of 0.065 ± 0.002 and 0.052 ± 0.003 respectively for the soft and hard bands. To characterize the presence of spectral variations, if any, we calculated the HR and show in Figure 2 a plot of HR against flux variations (in the units of counts s^{-1}) in the total (3–79 keV) band. A fit of a linear function of the form HR = m × counts s^{-1} (3–79) keV + c, which also takes into consideration the errors in both HR and the 3–79 keV count rates, gave values of -0.019 ± 0.005 and 0.465 ± 0.022 for m and c respectively. The spectrum is thus found not to change with the brightness of the source.

3.2. Spectral Analysis

Analysis of the spectrum of 3C 120 along with model fittings was carried out using the *XSPEC* package. To find the best-fit models, the χ^2 minimization technique in *XSPEC* was used.

Analysis of X-ray spectra is generally attempted by fitting simple phenomenlogical models such as the simple power-law model as well as the power law with exponential cut-off. Using power-law fits, Rani & Stalin (2018) obtained a value of $\Gamma = 1.85 \pm 0.01$. Similarly, using the *pexrav* model, the same authors obtained the value of the high-energy cut-off ($E_{\rm cut}$) to be 83^{+10}_{-8} keV. However, these models are too simplistic. Also, the power law with exponential cut off that is incorporated in *pexrav* has limitations in its approximation of the steep decline of the true high-energy cut off (Zdziarski et al. 2003; Fabian et al. 2015; Lubiński et al. 2016). Thus, both models are too simplistic to apply to the high-quality data from *NuSTAR* that are analyzed here. Therefore, the following more physical models were fit to the data.

3.2.1. CompTT Model

We used the Comptonization model (CompTT; Titarchuk 1994) convolved with a reflection component so as to get the coronal parameters. This model has the form TBabs × zTBabs× (zgauss+CompTT+refl(CompTT)). The first component of this model TBabs (Wilms et al. 2000) includes galactic absorption, with the galactic neutral hydrogen column density frozen to the value of 1.11×10^{21} cm^{-2} obtained from Dickey & Lockman (1990) using the nH tool in HEASARC[1], and the second component, zTBabs, represents absorption intrinsic to the host galaxy of the source. Redshift was fixed to $z = 0.033$ and the column density of zTBabs was kept as a free parameter in the fitting. The CompTT component in this model assumes a geometry for the corona (a slab or spherical) and models the intrinsic coronal continuum, and refl convolves it with reflection features (Baloković 2015). For a slab geometry the reduced χ^2 was 0.986 ($\chi^2/\nu = 3734/3788$) and for a spherical geometry it was also 0.986 ($\chi^2/\nu = 3734/3788$). For the slab geometry, we found a mean value of $kT_e = 9^{+2}_{-3}$ keV and $\tau = 2.4^{+0.6}_{-1.1}$ considering primary and reflected emission at 90% confidence. For the spherical geometry the best fit yielded a mean value of $kT_e = 16^{+6}_{-7}$ keV and $\tau = 5.1^{+0.6}_{-0.4}$ for primary and reflected emission at the 90% confidence. The CompTT model gave huge error bars in the normalization constant. The observed spectrum along with the fit and residuals are shown in Figure 3 for the spherical geometry and Figure 4 for the slab geometry. The best-fit parameters and their errors at 90% confidence levels are given in Table 1. The 2−10 keV flux determined from the fit is $(5.19 \pm 0.01) \times 10^{-11}$ erg cm^{-2} s^{-1}. This gives an unabsorbed luminosity of $(1.29 \pm 0.01) \times 10^{44}$ erg s^{-1}. Using the bolometric correction of 20.6 ± 0.1 found by Vasudevan & Fabian (2009) we obtained a bolometric luminosity of $(26.656 \pm 0.001) \times 10^{44}$ erg s^{-1}. For a black hole mass of 5.6×10^7 $M_\odot$ (Bentz & Katz 2015), the calculated Eddington accretion rate is $\lambda_{\rm Edd} = L_{\rm bol}/L_{\rm Edd} = 0.353$, where the Eddington luminosity, $L_{\rm Edd} = 1.36 \times 10^{38}$ $(M_{\rm BH}/M_\odot)$ erg s^{-1}. This is similar to the value of $\lambda_{\rm Edd} = 0.352$ found by Lubiński et al. (2016) using data from many telescopes including *INTEGRAL*.

3.2.2. CompPS

Although the CompTT model well represents the observed spectrum, it has limitations such as its simplistic treatment of the seed photons that participate in the Comptonization process. We therefore fit the spectrum using one of the most advanced Comptonization models available in *XSPEC*, namely CompPS (Poutanen & Svensson 1996). CompPS, which produces the continuum through thermal Comptonization processes, incorporates a proper treatment of the Comptonization process through exact numerical solution of the radiative transfer equations. It also offers several choices for the geometries. In the fitting process, when all the parameters were kept free, the fitting failed to converge. Therefore, to avoid non-convergence owing to the presence of many free parameters in CompPS fitting, we fixed the centroid energy and

[1] https://heasarc.gsfc.nasa.gov/cgi-bin/Tools/w3nh/w3nh.pl

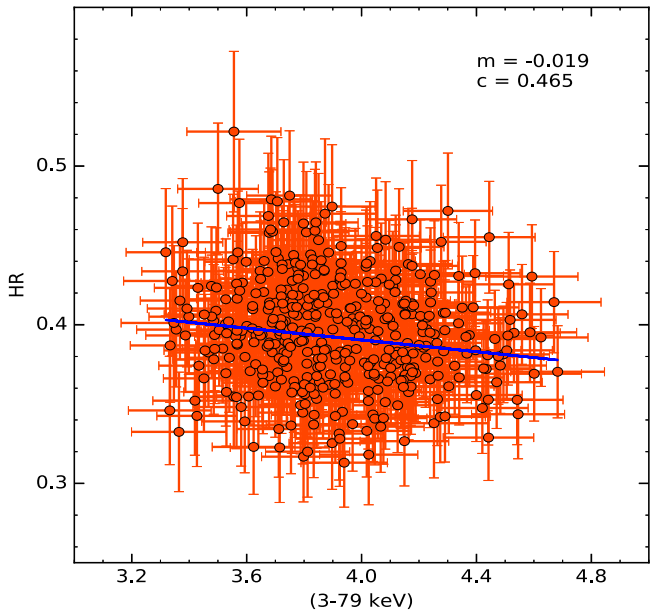

Figure 2. Correlation between HR and count rate variation in the 3−79 keV band. The solid blue line is the linear least-squares fit to the data.

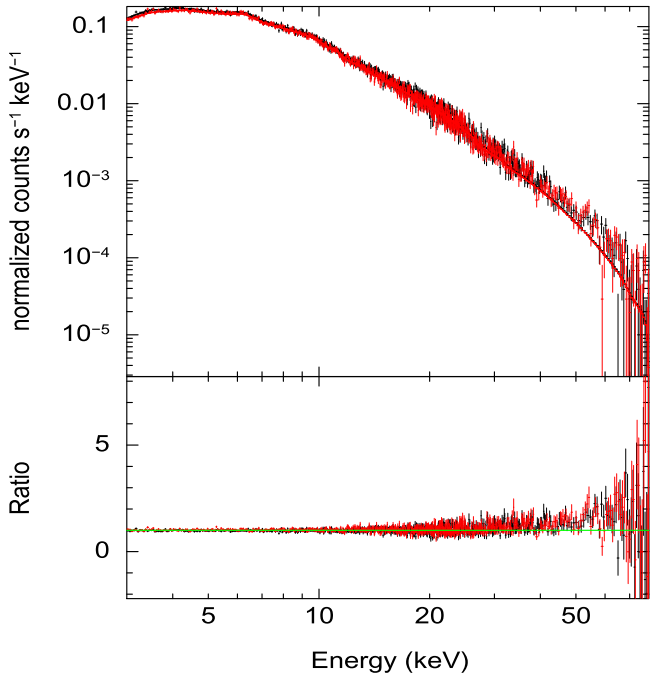

Figure 3. Observed spectrum (normalized counts s^{-1} vs. energy) along with the fitted model TBabs*ZTBabs*(zgauss+compTT+refl(compTT)) (for a spherical geometry) in FPMA (black) and FPMB (red). The ratio of observations to the fitted model is also shown for FPMA (black) and FPMB (red).

deviation of the Fe Kα line to be 6.43 keV and 0.29 keV respectively, obtained from CompTT for a slab geometry. The parameters obtained from the fit along with their associated errors including the Compton y parameter ($y = 4\tau\frac{KT}{m_e c^2}$, where τ is the Thomson optical depth; Zdziarski et al. 2000) and the normalization ($N_{\rm CompPS}$) are given in Table 1. To compare our results with CompTT, we used CompPS only for slab and spherical geometries. The seed photons were assumed to be 10 eV. The observed spectra along with the fit and residuals are

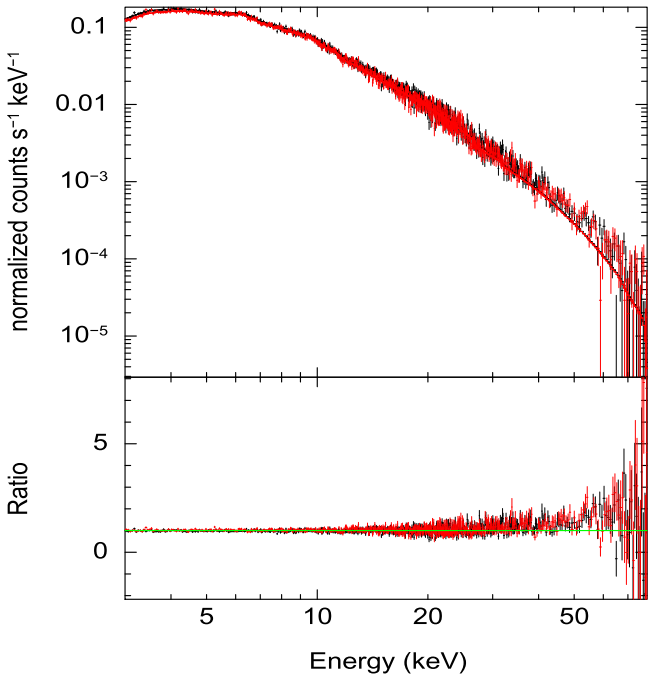

Figure 4. Same as in Figure 3 except for the slab geometry.

shown in Figure 5 for the spherical and the slab geometries. For the slab geometry we obtained a reduced ($\chi^2/\nu = 3773/3790$) of 0.996 whereas, for the spherical geometry the reduced ($\chi^2/\nu = 3783/3790$) was 0.998. For the slab and spherical geometry, we found R values of $0.80^{+0.11}_{-0.10}$ and 0.43 ± 0.06 respectively. We found that the kT_e values obtained from CompPS is larger than that obtained from CompTT for both spherical and slab geometries.

3.2.3. EQPAIR

The models used above to fit the *NuSTAR* data of 3C 120 assumes that the electrons involved in the Comptonization process are thermal electrons with a Maxwellian energy distribution. However, hybrid models for the corona that involve the contribution of both thermal and non-thermal electrons have been applied to AGNs. For example, in NGC 4151, the contribution of non-thermal electrons is found to be less than 15% (Zdziarski et al. 1996; Johnson et al. 1997). The non-thermal fraction can also be as large as 30% (Fabian et al. 2017). 3C 120 is known to have a jet emission (Eracleous & Halpern 1998) and it is likely the observed X-ray emission is a combination of various components. We therefore model the spectrum with the EQPAIR model (Coppi 1999), the most advanced Comptonization model in XSPEC. This model evaluates the emission spectrum resulting from Comptonization, Coulomb collisions, and pair production. This model can treat Comptonization for a different plasma nature (thermal, non-thermal, and hybrid) and even incorporate the Compton hump from cold reflection. This is because, in EQPAIR, only electrons with optical depth (τ_p) are accelerated with total power characterized by the compactness parameter l_h (such that $l_h = L_h\sigma_T/Rm_e c^2$, where L_h is the luminosity or the power supplied to the electrons in the Comptonization region and R the size of the Comptonization region; Done & Gierliński 2003) that is split between thermal distribution with power ($l_{\rm th}$) and non-thermal distribution with power $l_{\rm nth}$ and $l_h = l_{\rm nth} + l_{\rm th}$.

Table 1
Best-fit Parameters and Errors (90% Confidence) Obtained from Spectral Fitting for Different Models

Model Name	Parameter Name (units)	Parameter Values	χ^2/dof
CompTT			
TBabs*zTbabs*(zgauss +CompTT+refl (CompTT))	E (keV)	6.43 ± 0.06	0.986
(Spherical geometry)	σ (keV)	$0.29^{+0.10}_{-0.09}$	
	$N_{\rm zgauss} \times 10^{-5}$	$5.50^{+1.05}_{-1.01}$	
	mean kT_e (keV)	16^{+6}_{-7}	
	mean τ	$5.1^{+0.6}_{-0.4}$	
	$N_{\rm CompTT} \times 10^{6}$	$3.58^{+234}_{-2.99}$	
	R	0.29 ± 0.07	
	$N_{\rm refl(CompTT)} \times 10^{-2}$	$2.82^{+2.63}_{-2.67}$	
CompTT			
TBabs*zTbabs*(zgauss +CompTT+refl (CompTT))	E (keV)	6.43 ± 0.06	0.986
(Slab geometry)	σ (keV)	$0.29^{+0.10}_{-0.09}$	
	$N_{\rm zgauss} \times 10^{-5}$	$5.41^{+1.63}_{-1.05}$	
	mean kT_e (keV)	9^{+2}_{-3}	
	mean τ	$2.4^{+0.6}_{-1.1}$	
	$N_{\rm CompTT} \times 10^{7}$	$1.17^{+590}_{-1.16}$	
	R	$0.30^{+0.07}_{-0.08}$	
	$N_{\rm refl(CompTT)} \times 10^{-2}$	$2.79^{+0.25}_{-0.23}$	
CompPS			
TBabs*zTbabs*(zgauss +CompPS)	E (keV)	6.43*	0.996
(Slab geometry)	σ (keV)	0.29*	
	kT_e (keV)	25 ± 2	
	Compton y parameter	2.2 ± 0.1	
	R	$0.80^{+0.11}_{-0.10}$	
	ξ	2.36×10^{-3} $^{+0.237}_{-0.003}$	
	$N_{\rm CompPS} \times 10^{+8}$	3.23 ± 0.03	
CompPS			
TBabs*zTbabs*(zgauss +CompPS)	E (keV)	6.43*	0.998
(Spherical geometry)	σ (keV)	0.29*	
	kT_e (keV)	26^{+2}_{-0}	
	Compton y parameter	$2.99^{+2.99}_{-0.18}$	
	R	0.43 ± 0.06	
	ξ	2.13×10^{-3} $^{+0.161}_{-0.002}$	
	$N_{\rm CompPS} \times 10^{+7}$	$5.26^{+0.49}_{-0.06}$	
EQPAIR			
TBabs*zTbabs*(zgauss +EQPAIR)	l_h/l_s	0.90 ± 0.32	1.047
	l_{nt}/l_h	0.78 ± 0.10	
	kT_e (keV)	23^{+1}_{-7}	
	τ_p	0.60 ± 0.08	
	R	0.19 ± 0.03	
	ξ	5.14 ± 11.15	
	$N_{\rm EQPAIR} \times 10^{-3}$	0.69 ± 0.03	

Note. In the CompPS model the parameters marked with * were fixed to the best-fit values obtained from CompTT for a slab geometry. The errors in the parameters obtained from EQPAIR are the 1σ errors returned by the model fits.

These electrons then cool either through Compton scattering of soft photons or through Coulomb collisions. The parameter that plays an important role in characterizing the overall spectral shape in EQPAIR is the parameter l_h/l_s. The soft compactness parameter (l_s) refers to the luminosity of the soft photons that is injected into the corona and the hard compactness parameter l_h refers to the power supplied to the accelerated electrons in the source. To model the observed spectrum with EQPAIR, we fixed the centroid energy of the Fe Kα emission line to the best-fit value found from CompTT above for a slab geometry. However, in EQPAIR the geometry is spherical and the photons are induced homogeneously throughout the spherical cloud. We assumed that the input source of soft photons in EQPAIR is *diskpn*, a blackbody spectrum (Gierliński et al. 1999) with a peak temperature of 10 eV. The seed photon distribution can be modified in the model by changing l_s which for this model fitting was fixed to 10. The inclination was fixed to 17 degrees and the iron abundance was taken to be solar. For the purpose of this modeling we considered the accelerated particles to be electrons from the thermal pool. The best-fit parameters are given in Table 1. The observed and fitted spectra along with the residuals are given in Figure 5. Similar to the CompPS and CompTT models, the fit of the data with EQPAIR also provides a good description of the data with a reduced χ^2 of $1.047(\chi^2/\nu = 3972/3791)$. However, the temperature is not among the default output parameters returned by EQPAIR, though it is calculated in the model. We therefore used the *chatter* command (*chatter* level = 15) (Coppi 1999) and obtained $kT_e = 23$. The error in kT_e was obtained using χ^2 minimization technique at the 90% significance level. Thus, using the EQPAIR model we found $kT_e = 23^{+1}_{-7}$ keV. We found the best-fit ratio of the hard to the soft compactness parameter, $l_h/l_s = 0.90 \pm 0.32$. This points to similar power in the irradiating soft photons that enter the source region and in the heating of the electrons. The EQPAIR model yielded the value of ionization parameter of the reflector to be $\xi = 5.14 \pm 11.15$. The electron optical depth obtained by the fit was $\tau_p = 0.60 \pm 0.08$. The ratio $l_{\rm nth}/l_h$, which gives the fraction of power supplied to energetic particles that goes into accelerating non-thermal particles, was found to be 0.78 ± 0.10. The value of $l_{\rm nth}/l_h$ is zero for a purely thermal model, while it is unity for a purely non-thermal model. Though $l_{\rm nth}/l_h$ obtained from the fit deviates greatly from zero, the detection of a high-energy cut off in the *NuSTAR* spectrum not much beyond the sensitivity of *NuSTAR* (Rani & Stalin 2018) and the non-detection of the source in γ-rays suggest that Comptonization by non-thermal electrons, if any, is non-significant. The χ^2 from the EQPAIR model fit is poorer than from CompPS and CompTT, although the kT_e value agrees with that obtained from CompPS. Thus, it is likely that in 3C 120, for the observations analyzed here, the electrons involved in the Comptonization process are predominantly thermal.

4. Discussion

4.1. Coronal Properties

The availability of high-quality *NuSTAR* data from observations of about 120 ks has enabled the determination of the coronal properties of 3C 120. The time-averaged spectrum covering the 3–79 keV band, when fitted with the phenomenological power-law model, gave a continuum power law index

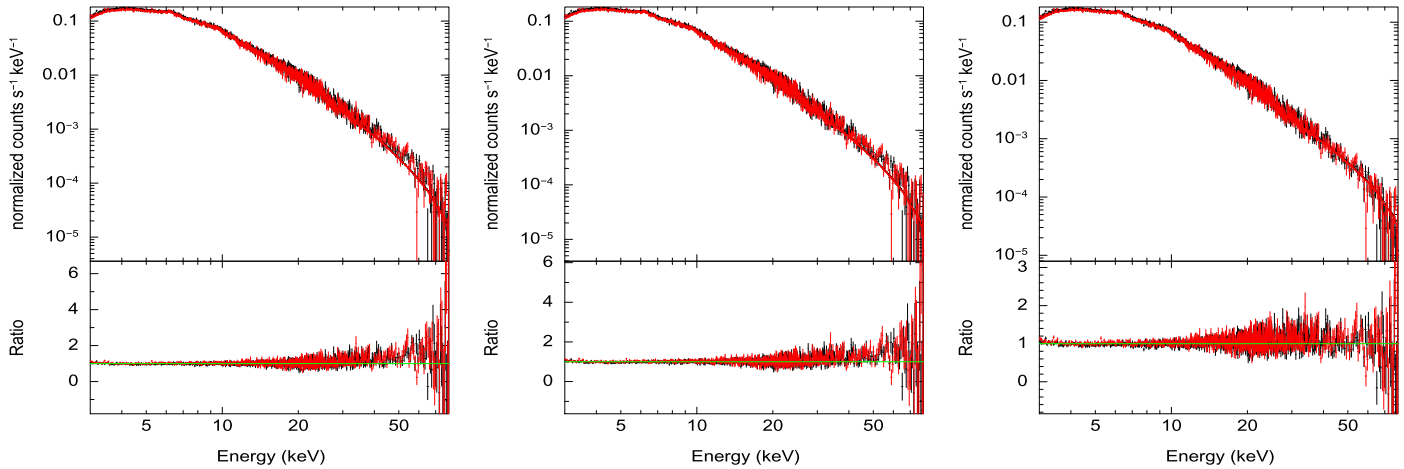

Figure 5. Left: observed spectrum (normalized counts s^{-1} vs. energy) along with the fitted model TBabs*zTbabs*(zgauss+compPS) (for a slab geometry) for FPMA (black) and FPMB (red). Middle: the same, except for the spherical geometry. Right: observed spectrum fitted with EQPAIR (TBabs*zTbabs*(zgauss+EQPAIR)).

of $\Gamma = 1.85 \pm 0.01$ (Rani & Stalin 2018). However, values of 1.70 and 2.08 were found from *XMM* (Vasudevan & Fabian 2009) and *INTEGRAL* (Lubiński et al. 2016) observations. From *BeppoSAX* observations, Zdziarski & Grandi (2001) found the continuum to be well described by a power law with $\Gamma \sim 1.85 \pm 0.05$, which is in close agreement with that found from *NuSTAR* data by Rani & Stalin (2018). The difference in the photon index values obtained from different sets of observations acquired from different telescopes could point to spectral variations in the source.

Using the *pexrav* model with the inclusion of a Gaussian component to account for the presence of the Fe Kα line in the spectrum, Rani & Stalin (2018) found values of $\Gamma = 1.87 \pm 0.02$ and $E_{\rm cut} = 83^{+10}_{-8}$ keV. 3C 120 has been observed before by *BeppoSAX* and OSSE. By modeling the *BeppoSAX* data with an e-folded power law or a thermal Comptonization model, Zdziarski & Grandi (2001) found a value of $E_{\rm cut} = 150^{+230}_{-30}$ keV. Using an *ASCA* observation that was contemporaneous with an OSSE observation, and modeling the spectra with a broken power law multiplied by an exponential factor, Wozniak et al. (1998) found $E_{\rm cut} = 110^{+130}_{-50}$ keV. Within error bars, the value of $E_{\rm cut}$ obtained from *NuSTAR* data using simple model fits matches with that known from *BeppoSAX* and OSSE data, but with improved precision, with a manifold reduction in the errors. As these observations were taken at different epochs, it is also likely the $E_{\rm cut}$ is variable, but this cannot be ascertained because of the large error bars in its values from earlier observations. The Fe Kα line is well fit by a Gaussian incorporated in CompTT with σ of $0.29^{+0.09}_{-0.10}$ keV and $0.29^{+0.09}_{-0.10}$ keV respectively for the slab and spherical geometry. This is much narrower than the value of $\sigma = 0.8$ keV obtained from *ASCA* observations (Grandi et al. 1997).

In this work, we applied physical models to the data in contrast to the simple phenomenological models used earlier to understand the spectral characteristics of 3C 120 (Zdziarski & Grandi 2001; Rani & Stalin 2018). We fitted CompTT to the observed spectrum and used it to characterize the temperature and optical depth of the electrons in the corona for two geometries, namely a sphere and a slab. The goodness of the fit (with a nearly identical chi-square per degree of freedom of $\chi^2/\nu \approx 3734/3788$) is found to be insensitive to the assumption of the coronal geometry as the assumption of both slab and spherical geometries fit the data equally well and we obtained $kT_e = 9^{+2}_{-3}$ keV for the former and $kT_e = 16^{+6}_{-7}$ keV for the latter. These two model assumptions about the geometry of the corona gave different values of the optical depth, with $\tau = 2.4^{+0.6}_{-1.1}$ and $\tau = 5.1^{+0.6}_{-0.4}$ for the slab and spherical geometry respectively. This is expected because the optical depth for a slab is measured vertically while for a sphere it is measured radially. Using CompPS, an advanced Comptonization model available in XSPEC, we found kT_e values of 25 ± 2 and 26^{+2}_{-0} for the slab and spherical geometry. Within errors, these values of kT_e match with those obtained from the fit of the EQPAIR model to the *NuSTAR* data, which returned a value of $kT_e = 23^{+1}_{-7}$ keV.

This value of kT_e is much lower than the value of 176 keV obtained by Lubiński et al. (2016). This discrepancy might be attributed to the presence of a significant jet contribution during the epoch of observations done from *INTEGRAL*.

Considering the CompPS model, the derived value of kT_e is nearly identical for both the slab and spherical geometry of the corona. This could mean that the shape of the X-ray spectra emerging from these two geometries is quite similar and the available spectral data from *NuSTAR* are not sufficient to distinguish between them.

4.2. Nature of the Corona in 3C 120

3C 120 is classified as a Seyfert 1 galaxy (Burbidge 1967) and is also identified as a BLRG by Walker et al. (1987). It has a one-sided jet and is also known to be a γ-ray emitter from *Fermi* data (Sahakyan et al. 2015; Tanaka et al. 2015), which provides additional evidence for the presence of a powerful relativistic jet, already seen in radio observations (Harris et al. 2004). It is known that BLRGs have harder X-ray spectra in comparison to radio-quiet Seyfert galaxies (Zdziarski & Grandi 2001). However, spectral fits to the *NuSTAR* data analyzed here by Rani & Stalin (2018) using the *pexrav* model, gave a photon index Γ of 1.87 ± 0.02. This value is similar to that known for non-jetted Seyfert 1 galaxies and different from the X-ray spectra of AGNs with relativistic jets (blazars) which have $\Gamma < 1.5$ (Sambruna et al. 2006; Gianní 2011). Though the derived X-ray spectral index points to negligible contribution of the jet emission, we checked for the signature of jets in our data by looking at the multi-wavelength properties during the epoch of *NuSTAR* observations. Using the light curves taken in

Table 2
Summary of the Physical Parameters of the AGNs taken from the Literature Obtained from *NuSTAR* Data

Name	Type	$E_{\rm cut}$ (keV)	kT$_e^a$	Γ	log ($M_{\rm BH}$)	$\lambda_{\rm Edd}$	References
3C 382	BLRG/Sy 1	214^{+147}_{-63}	330 ± 30	$1.68^{+0.03}_{-0.02}$	9.2 ± 0.5	0.109	1
3C 390.3	BLRG/Sy 1	116^{+24}_{-8}	16^{+4}_{-2}	1.70 ± 0.01	8.4 ± 0.1	0.240	2
IC 4329A	Sy 1.2	186^{+14}_{-14}	50^{+6}_{-3}	1.73 ± 0.01	6.8 ± 0.2	0.082	3
MCG-5-23-16	NELG/Sy 2	116^{+6}_{-5}	25 ± 2	1.85 ± 0.01	7.8 ± 0.2	0.031	4
NGC 5506	Sy 1.9	720^{+130}_{-190}	...	1.91 ± 0.03	8.0 ± 0.2	0.013	5
J2127.4+5654	NLSy1	108^{+11}_{-10}	53^{+28}_{-26}	2.08 ± 0.01	7.2 ± 0.0	0.090	6
GRS 1734-292	Sy 1	53^{+11}_{-8}	$12.1^{+1.8}_{-1.2}$	1.65 ± 0.05	8.5 ± 0.1	0.033	7
4C 74.26	BLRG/Sy 1	183^{51}_{-35}	46^{+25}_{-11}	$1.84^{+0.03}_{-0.02}$	9.6 ± 0.5	0.037	8
Ark 564	NLSy1	42^{+3}_{-3}	15^{+2}_{-1}	2.27 ± 0.08	6.4 ± 0.5	1.10	9
QSO B2202-209	RQQ	153^{+103}_{-54}	42 ± 3	1.82 ± 0.05	9.1 ± 0.2	1.15	10
NGC 5273	Sy 1.5	143^{+96}_{-40}	57^{+18}_{-11}	2.27 ± 0.08	6.4 ± 0.5	1.1	11
3C 120	BLRG/Sy 1	83^{+10}_{-8}	26^{+2}_{-0}	1.87 ± 0.02	7.7 ± 0.1	0.353	This work

Note. Column 1 gives the name of the source, column 2 gives the type of the source, column 3 gives the cut-off energy in keV, column 4 is the plasma temperature of the corona for a spherical geometry, column 5 is the photon index, column 6 is the logarithm of the black hole mass in solar mass units, column 7 is the Eddington accretion rate, and column 8 gives the references to the sources from where their physical parameters were taken.
References. 1. Ballantyne et al. (2014), 2. Lohfink et al. (2015), 3. Brenneman et al. (2014b), 4. Brenneman et al. (2014b), 4. Baloković (2015), 5. Matt et al. (2015), 6. Marinucci et al. (2014), 7. Tortosa et al. (2017), 8. Lohfink et al. (2017); Woo & Urry (2002), 9. Vasudevan & Fabian (2007); Kara et al. (2017) 10. Kammoun et al. (2017) 11. Pahari et al. (2017) [a] the quoted kT_e values for the sources except NGC 5273 pertain to spherical geometry. For 3C 120 the quoted value is that returned by the CompPS model fit.

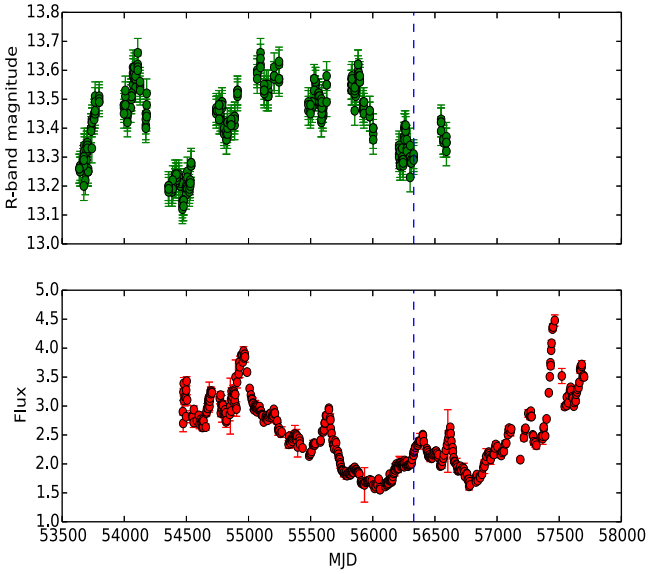

Figure 6. Long-term optical V-band light curves from CRTS (top panel) and 15 GHz radio light curves from OVRO (bottom panel). The epoch of *NuSTAR* observation studied here is indicated by the blue dashed line.

the optical from the Catalina Realtime Transient Survey (CRTS; Drake et al. 2009) and in the 15 GHz band in the radio from the Owens Valley Radio Observatory (OVRO; Richards et al. 2011), we found that 3C 120 was in a moderately low flux state during the time of *NuSTAR* observation analyzed here. The optical and radio light curves are given in Figure 6 with the epoch of *NuSTAR* observations indicated as a blue dashed line. Also, during the epoch of the *NuSTAR* observations used here, the source was not detected in γ-rays by *Fermi* (Tanaka et al. 2015). The $F_{\rm var}$ values for 3C 120 in the soft and hard bands are 0.065 ± 0.002 and 0.052 ± 0.003 respectively. This is much lower than the average $F_{\rm var}$ in X-rays shown by the blazar class of AGNs (Soldi et al. 2014; Rani et al. 2017) Also, the variations seen in the *NuSTAR* data are similar to those of Seyfert galaxies and not blazars (Rani et al. 2017). Model fits to the observed spectrum using CompPS that considered thermal Comptonization gave a value of $kT_e = 26^{+2}_{-0}$ keV for a spherical geometry. On the other hand, fits to the observed spectrum using EQPAIR that treats Comptonization from a hybrid plasma gave $kT_e = 23^{+1}_{-7}$ keV. Comparing CompTT and CompPS for a spherical geometry using an F-test we find an F-value of 1.013. The test does not rule out the null hypothesis that the two chi-square distributions are the same at the 90% confidence level. Between the CompPS and EQPAIR model fits for a spherical geometry we find an F-value of 1.0637, larger than the $F_{\rm critical}$ value for a 90% confidence level, rejecting the null hypothesis that the two chi-square distributions are the same. As the chi-square value of CompPS is closer to unity compared to EQPAIR, we consider that CompPS better represents the spectrum of 3C 120. Therefore, based on both spectral (presence of the X-ray high-energy cut-off and the X-ray photon index being close to that known for Seyfert galaxies) and timing analysis (non-detection of the source in γ-rays during the epoch of *NuSTAR* observations), it is clear that the X-rays observed by *NuSTAR* from 3C 120 are similar to those found in non-jetted Seyfert 1 galaxies considering a model of a thermal Comptonizing corona producing the X-rays in 3C 120. We note that the strength of the reflection component obtained here showed significant differences between various model fits, which might the due to the low S/N of the data beyond 30 keV.

4.3. Comparison with the Coronal Properties of Other AGNs

Because of the degeneracies involved in the evaluation of the properties of the corona from the observed X-ray spectrum, we need to simultaneously measure the power-law slope and the cut-off energy. This demands high-quality X-ray spectra. Measurements of $E_{\rm cut}$ are known for several AGNs from observatories such as *BeppoSAX* and *INTEGRAL*. However, most of these measurements have large error bars. Recently,

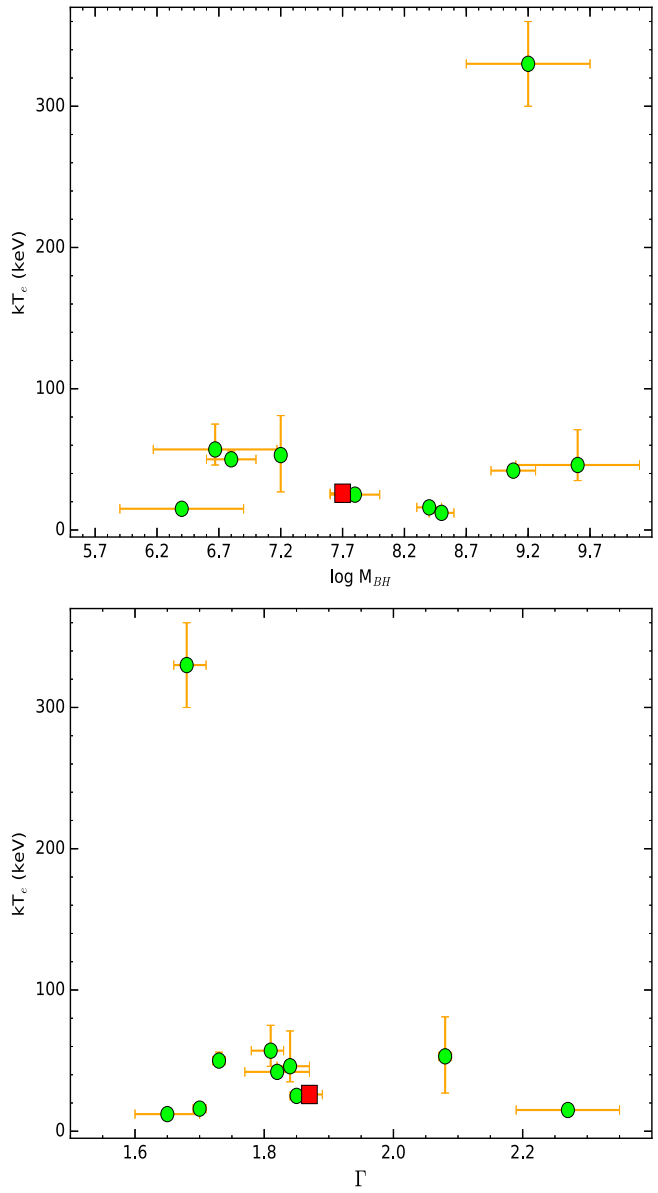

Figure 7. Correlation between kT_e in keV and logarithm of $M_{\rm BH}$ in units of $M_\odot$ (top panel) and Γ (bottom panel) for the sample of sources culled from the literature with known $E_{\rm cut}$ measurements from *NuSTAR* (without lower limits). 3C 120 is shown as a red square.

observations from *NuSTAR* have started to provide reliable estimates of $E_{\rm cut}$ in a few AGNs, even though it might not be sensitive to sources with $E_{\rm cut}$ much larger that its spectral coverage.

To compare the coronal measurements reported here for 3C 120 with those of other AGNs, we searched the literature for the availability of coronal properties of AGNs based on observations either from *NuSTAR* alone or *NuSTAR* observations coupled with other telescopes. Focusing only on those sources that have $E_{\rm cut}$ measurements (without lower limits) we arrived at a sample of 12 sources including 3C 120. They are given in Table 2. Also, the sources listed in Table 2 belong to different types of AGN that include both radio-quiet Seyferts and BLRGs (3C 390.3 and 3C 120, 3C 282 and 3C 390.3). Analysis of a larger sample of AGNs does indicate differences between BLRGs and radio-quiet Seyfert 1 galaxies, with BLRGs having, on average, lesser Compton reflection, a weaker Fe Kα line, and harder hard X-ray spectra compared to radio-quiet Seyfert 1 galaxies (Wozniak et al. 1998). These differences are further confirmed by Zdziarski & Grandi (2001); however, the authors state that the distribution of these parameters in these two populations of sources is not distinct. They obtained mean values of $\Gamma = 1.74 \pm 0.04$ and 1.95 ± 0.05 for BLRGs and radio-quiet Seyferts, respectively. The value of Γ obtained for 3C 120 by Rani & Stalin (2018) is closer to what is known for radio-quiet Seyfert 1 galaxies and is steeper than the other two BLRGs 3C 282 and 3C 390.3. This also supports the dormant state of the jet of 3C 120 during the epoch of *NuSTAR* observations reported here. Though the kT_e values of 3C 120 and 3C 390.3 agree within a factor of two, the value of kT_e obtained for 3C 382, another BLRG, is much larger. Therefore, based on existing data from *NuSTAR*, it is very difficult to say if the coronal properties of radio-loud AGNs (BLRGs) and radio-quiet AGNs (radio-quiet Seyfert 1 galaxies) are similar or different. Understanding the connection between radio-emission and coronal properties, if any, needs observations on a large number of sources of both types analyzed in a homogeneous manner. For this modest sample of sources with *NuSTAR* observations culled from the literature, we looked for correlation of kT_e with other physical parameters of the sources, such as Γ and the black hole mass. No correlation could be established (Figure 7). Therefore, more measurements of kT_e on a large sample that comprises both radio-loud and radio-quiet AGNs are required to determine the existence or absence of such correlations and largely to better understand the nature of the corona in AGNs.

5. Summary

We have carried out timing and spectral analysis of the Seyfert 1 galaxy 3C 120 using ∼120 ks observations from *NuSTAR*. The results of our analysis are summarized below.

1. The source showed variations in the count rates during the duration of the X-ray observations. The amplitudes of count rate variations characterized by $F_{\rm var}$ are found to be 0.065 ± 0.002 and 0.052 ± 0.003 for the soft (3–10) keV and the hard (10–79) keV bands respectively, thus showing more variation in the soft band relative to the hard band.
2. The X-ray spectrum characterized by HR is found not to show a correlation with the flux variations in the total band, indicating the spectrum was non-variable during the epoch of *NuSTAR* observation.
3. From a fit of the CompTT model to the time-averaged spectrum we found evidence for the presence of a weak Fe Kα line in the data at 6.4 keV with an equivalent width of 60 ± 5 eV. The line is best fit by a Gaussian with a σ of 0.29 keV.
4. Using the Comptonization model CompPS to fit the observed spectrum, we derived the kinetic temperature of the coronal electrons to be $kT_e = 25 \pm 2$ keV with a Compton y parameter of $y = 2.2 \pm 0.2$ for a slab geometry. This is similar to the value of the kinetic temperature of $kT_e = 26^{+2}_{-0}$ keV obtained for a spherical geometry with a y of $2.99^{+2.99}_{-0.18}$. Also, fitting the observed spectrum with EQPAIR gave a best-fit value of $kT_e = 23^{+1}_{-7}$ keV. Thus, fits to the data with the two most advanced Comptonization models available in *XSPEC*, namely CompPS and EQPAIR, gave similar values of

coronal temperature. It is likely that the electrons participating in the Comptonization process is predominantly thermal. Comptonization by non-thermal electrons, if any, is insignificant as (i) the source is not detected in γ-rays during the epoch of *NuSTAR* observations, and (ii) the X-ray photon index is similar to that known for Seyfert galaxies.

5. 3C 120 is known to have a large-scale radio jet and is also a γ-ray emitter. However, *NuSTAR* data analyzed here have made it possible to detect coronal spectral signatures, and constrain kT_e and the reflection features, which are found to be similar to those known for radio-quiet Seyfert galaxies. This indicates that the contribution of jet emission to the X-ray is negligible in the *NuSTAR* data and is likely to be weak during the epoch of *NuSTAR* observations. Additional support for this is provided by the similar values of kT_e obtained by both the CompPS and EQPAIR model fits to the *NuSTAR* observations. This is also supported by the low/moderate radio and optical flux states as well as non-detection by *Fermi* during the epoch of *NuSTAR* observations. To constrain the contribution of jet emission, if any, to the X-ray emission from 3C 120 requires observations at energies higher than those covered by *NuSTAR*.

We thank the referee for his/her critical and valuable comments that improved the paper significantly. This research made use of data from the *NuSTAR* mission, a project led by the California Institute of Technology, managed by the Jet Propulsion Laboratory, and funded by NASA, XMM-Newton, an ESA science mission with instruments and contributions directly funded by ESA Member States and NASA. This research has made use of the *NuSTAR* Data Analysis Software (NuSTARDAS) jointly developed by the ASI Science Data Center (ASDC, Italy) and the California Institute of Technology (USA).

ORCID iDs

Priyanka Rani https://orcid.org/0000-0002-8448-5361

References

Abdo, A. A., Ackermann, M., Ajello, M., et al. 2010, ApJ, 720, 912
Acero, F., Ackermann, M., Ajello, M., et al. 2015, ApJS, 218, 23
Anders, E., & Grevesse, N. 1989, GeCoA, 53, 197
Arnaud, K. A. 1996, in ASP Conf. Ser. 101, Astronomical Data Analysis Software and Systems V, ed. G. H. Jacoby & J. Barnes (San Francisco, CA: ASP), 17
Ballantyne, D. R., Bollenbacher, J. M., Brenneman, L. W., et al. 2014, ApJ, 794, 62
Baloković, M., Matt, G., Harrison, F. A., et al. 2015, ApJ, 800, 62
Balucinska-Church, M., & McCammon, D. 1992, ApJ, 400, 699
Bentz, M. C., & Katz, S. 2015, PASP, 127, 67
Brenneman, L. W., Madejski, G., Fuerst, F., et al. 2014a, ApJ, 781, 83
Brenneman, L. W., Madejski, G., Fuerst, F., et al. 2014b, ApJ, 788, 61
Burbidge, E. M. 1967, ApJL, 149, L51
Coppi, P. S. 1999, in ASP Conf. Ser. 161, High Energy Processes in Accreting Black Holes, ed. J. Poutanen & R. Svensson (San Francisco, CA: ASP), 375
Dadina, M. 2007, A&A, 461, 1209
Dickey, J. M., & Lockman, F. J. 1990, ARA&A, 28, 215
Done, C., & Gierliński, M. 2003, MNRAS, 342, 1041
Drake, A. J., Djorgovski, S. G., Mahabal, A., et al. 2009, ApJ, 696, 870
Edelson, R., Turner, T. J., Pounds, K., et al. 2002, ApJ, 568, 610
Eracleous, M., & Halpern, J. P. 1998, ApJ, 505, 577
Fabian, A. C., Lohfink, A., Belmont, R., Malzac, J., & Coppi, P. 2017, MNRAS, 467, 2566
Fabian, A. C., Lohfink, A., Kara, E., et al. 2015, MNRAS, 451, 4375
Fabian, A. C., Zoghbi, A., Ross, R. R., et al. 2009, Natur, 459, 540
Fanaroff, B. L., & Riley, J. M. 1974, MNRAS, 167, 31P
George, I. M., & Fabian, A. C. 1991, MNRAS, 249, 352
Gianní, S., de Rosa, A., Bassani, L., et al. 2011, MNRAS, 411, 2137
Gierliński, M., Zdziarski, A. A., Poutanen, J., et al. 1999, MNRAS, 309, 496
Grandi, P., Sambruna, R. M., Maraschi, L., et al. 1997, ApJ, 487, 636
Haardt, F., & Maraschi, L. 1991, ApJL, 380, L51
Haardt, F., Maraschi, L., & Ghisellini, G. 1994, ApJL, 432, L95
Haardt, F., Maraschi, L., & Ghisellini, G. 1997, ApJ, 476, 620
Halpern, J. P. 1985, ApJ, 290, 130
Harris, D. E., Mossman, A. E., & Walker, R. C. 2004, ApJ, 615, 161
Harrison, F. A., Craig, W. W., Christensen, F. E., et al. 2013, ApJ, 770, 103
Johnson, W. N., Kinzer, R., Kurfess, J. D., et al. 1993, ApJS, 86, 693
Johnson, W. N., McNaron-Brown, K., Kurfess, J. D., et al. 1997, ApJ, 482, 173
Kammoun, E. S., Risaliti, G., Stern, D., et al. 2017, MNRAS, 465, 1665
Kara, E., García, J. A., Lohfink, A., et al. 2017, MNRAS, 468, 3489
Lin, Y. C., Bertsch, D. L., Dingus, B. L., et al. 1993, ApJL, 416, L53
Lohfink, A. M., Fabian, A. C., Ballantyne, D. R., et al. 2017, ApJ, 841, 80
Lohfink, A. M., Ogle, P., Tombesi, F., et al. 2015, ApJ, 814, 24
Lubiński, P., Beckmann, V., Gibaud, L., et al. 2016, MNRAS, 458, 2454
Malizia, A., Molina, M., Bassani, L., et al. 2014, ApJL, 782, L25
Marinucci, A., Matt, G., Kara, E., et al. 2014, MNRAS, 440, 2347
Marinucci, A., & Tortosa, A. 2016, AN, 337, 490
Matt, G., Baloković, M., Marinucci, A., et al. 2015, MNRAS, 447, 3029
Miller, J. M. 2007, ARA&A, 45, 441
Nolan, P. L., Abdo, A. A., Ackermann, M., et al. 2012, ApJS, 199, 31
Pahari, M., McHardy, I. M., Mallick, L., Dewangan, G. C., & Misra, R. 2017, MNRAS, 470, 3239
Perola, G. C., Matt, G., Cappi, M., et al. 2002, A&A, 389, 802
Petrucci, P. O., Haardt, F., Maraschi, L., et al. 2001, ApJ, 556, 716
Poutanen, J., & Svensson, R. 1996, ApJ, 470, 249
Rani, P., & Stalin, C. S. 2018, JApA, in press (doi:10.1007/s12036-017-9502-5)
Rani, P., Stalin, C. S., & Rakshit, S. 2017, MNRAS, 466, 3309
Rees, M. J. 1984, ARA&A, 22, 471
Richards, J. L., Max-Moerbeck, W., Pavlidou, V., et al. 2011, ApJS, 194, 29
Sahakyan, N., Zargaryan, D., & Baghmanyan, V. 2015, A&A, 574, A88
Sambruna, R. M., Markwardt, C. B., Mushotzky, R. F., et al. 2006, ApJ, 646, 23
Shakura, N. I., & Sunyaev, R. A. 1973, A&A, 24, 337
Soldi, S., Beckmann, V., Baumgartner, W. H., et al. 2014, A&A, 563, A57
Tanaka, Y., Nandra, K., Fabian, A. C., et al. 1995, Natur, 375, 659
Tanaka, Y. T., Doi, A., Inoue, Y., et al. 2015, ApJL, 799, L18
Titarchuk, L. 1994, ApJ, 434, 570
Tortosa, A., Marinucci, A., Matt, G., et al. 2017, MNRAS, 466, 4193
Urry, C. M., & Padovani, P. 1995, PASP, 107, 803
Vasudevan, R. V., & Fabian, A. C. 2007, MNRAS, 381, 1235
Vasudevan, R. V., & Fabian, A. C. 2009, MNRAS, 392, 1124
Vaughan, S., Edelson, R., Warwick, R. S., & Uttley, P. 2003, MNRAS, 345, 1271
Walker, R. C., Benson, J. M., & Unwin, S. C. 1987, ApJ, 316, 546
Wilms, J., Allen, A., & McCray, R. 2000, ApJ, 542, 914
Woo, J.-H., & Urry, C. M. 2002, ApJ, 579, 530
Wozniak, P. R., Zdziarski, A. A., Smith, D., Madejski, G. M., & Johnson, W. N. 1998, MNRAS, 299, 449
Zdziarski, A. A., & Grandi, P. 2001, ApJ, 551, 186
Zdziarski, A. A., Johnson, W. N., & Magdziarz, P. 1996, MNRAS, 283, 193
Zdziarski, A. A., Lubiński, P., Gilfanov, M., & Revnivtsev, M. 2003, MNRAS, 342, 355
Zdziarski, A. A., Poutanen, J., & Johnson, W. N. 2000, ApJ, 542, 703
Zensus, J. A. 1989, in BL Lac Objects, ed. L. Maraschi, T. Maccacaro, & M.-H. Ulrich (Berlin: Springer), 3